MODELLING OF A BST-0.5 IDC WITH APPLICATION IN ELECTRONICALLY SCANNED CRLH LWA

S. Ramezanpour*, S. Nikmehr, and A. Poorziad

Department of Electrical and Computer Engineering, University of Tabriz, 29 Bahman Boulevard, Tabriz, Iran

Abstract—Modeling of a ferroelectric interdigital capacitor (IDC) and its incorporating in composite right/left-handed (CRLH) unit cells is represented. To evaluate the capacitance of a multi-layered IDC structures, conformal mapping and partial capacitance methods are utilized. Furthermore, the partial displacement method is utilized to calculate the electric field distribution and the its relation in the ferroelectric layer to applied voltage is obtained. Using this relation in a phenomenological model, dependency of the relative permittivity of ferroelectric on the applied voltage is obtained. The designed unit cell is comprised of IDCs and spiral inductors. To alter the propagation constant of the unit cell by varying the applied voltage, a thin layer of $Ba_{0.5}Sr_{0.5}TiO_3$ (BST-0.5) ferroelectric is incorporated underneath an IDC, called BST-0.5 varactor. The periodic structure based on the designed unit cell leads to a CRLH LWA. The Tunability of the periodic structure with three unit cell is demonstrated by varying the relative permittivity of the ferroelectric layer.

1. INTRODUCTION

The theory of CRLH MTM describes dual right-handed (RH)/left-handed (LH) nature of metamaterials. The continuous transition from LH to RH, in the dispersion curve of a CRLH MTM, is called the balanced condition. The periodic structure of CRLH unit cells in the balanced condition leads to a CRLH LWA [1]. The CRLH transmission line can also be bent into a circle to realize a ring antenna [2].

Many CRLH LWA structures have already been represented in research articles. In Ref. [3], an improved CRLH unit was presented in which the parasitic self-resonances of the capacitor were shifted outside

* Corresponding author: Shahab Ramezanpour (shahabramezanpour@yahoo.com).

of the operational frequency band and, thus, the radiation range was extended. In [4], a double-side radiating LWA based on CRLH coplanar-waveguide (CPW) was proposed. [5] presented a realization of CRLH transmission lines using coupled microstrip lines.

A CRLH LWA is a frequency dependent structure, however modern communication systems, generally require fixed frequency operations which can be obtained by varying LC parameters. A different approach was utilized in Ref. [6] in which an open waveguide was filled with a bulk ferrite material and the propagation constant of the structure was varied by magnetic field bias voltage. However, in most application, thin film material for compatibility with MIC technology and also electric field bias was preferred [7].

Tuning LC parameters at a fixed frequency can be obtained by incorporating varactor diodes [8] and/or tunable inductor chips [9] along the structure. In comparison with varactor diodes, variable capacitors using thin film ferroelectric materials have low cost, high speed and integration capability with MMICs [10]. Tunable capacitors using $Ba_xSr_{1-x}TiO_3$ thin film, called BST varactors, have two conventional structures; parallel plates (metal-insulator-metal (MIM)) and interdigital capacitors (IDC). IDC varactors require higher tuning voltage compared to MIMs, therefore, they are less sensitive to ac voltages. In addition, unlike MIMs, they require only one level of metallization [11]. In this paper a tuned interdigital capacitor with thin film BST-0.5 is utilized. An IDC is comprised of coplanar strips (CPS). Various methods have been proposed to analyse CPS lines. In [12], simple and accurate models based on artificial neural networks (ANNs) were presented to determine the physical dimensions of CPS lines. In [13], the definition of characteristic impedance for lossless microstrip and coplanar lines was considered by calculating the displacement current related to longitudinal component of the electric field. In [14], conformal mapping and Schwartz-Christoffel transformation were utilized to analyse CPS lines.

This paper is comprised of four main sections. Section 2 represents a proposed method to evaluate the capacitance of the periodic section of an IDC. Furthermore, a formula is derived for the effective length of the fringing capacitor. In Section 3, the relation of the electric field in the ferroelectric layer with the applied voltage is derived. Using this relation in a phenomenological model, the dependency of the ferroelectric layer's relative permittivity to the applied voltage is obtained. A design procedure for a modified CRLH unit cell, incorporating BST-0.5 IDCs, is covered in Section 4. The construction of periodic structure, based on the designed unit cell, is carried out in Section 5 and its tunability is shown by varying the relative

permittivity of the ferroelectric layer.

2. MULTILAYERED STRUCTURE OF AN IDC

2.1. Capacitance Calculation

Here, a simplified method of analysis, based on physical insight, is proposed for the periodic section of the IDC. The layout of an IDC is shown in Fig. 1, in which $2s$, $2g$, $2g_e$, ℓ, $2w$ and $n = 6$ stand for finger width, gap between fingers, gap at end of fingers, overlapping length, electrode width and number of fingers, respectively. The total capacitance of an IDC can be expressed as [14],

$$C = C_3 + C_n + C_{end} \tag{1}$$

where, C_n, C_3, and C_{end} are the capacitance of periodical structure, the capacitance of three remaining fingers, and fringing capacitance created at the end of fingers, respectively. The structure to calculate the capacitance of periodical section along with its division into three sub-structures, according to the partial capacitance method, is depicted in Fig. 2. General form of sub-structures of Fig. 2 is shown in Fig. 3, where for simplifying the analyses, the magnetic walls at both ends (defined in [14]) are moved to infinity without any influence on the field line distributions (magnetic walls are shown by dotted lines). Note that, in the Ref. [14], unlike to our method of the magnetic walls movement to infinity, an approximate transformation is utilized to calculate the capacitance. Our procedure to calculate the capacitance C_n of Fig. 3 is given in Appendix A, while we have used the method of [14] in calculating C_3 and C_{end}. In order to validate our method
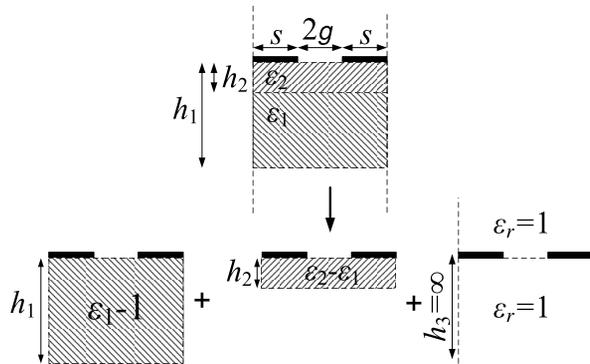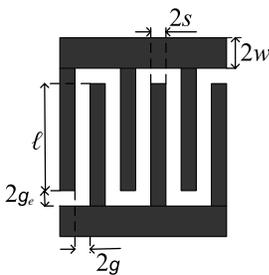
Figure 1. Layout of an IDC.

Figure 2. Periodical section of an IDC and its division into three sub-structures.
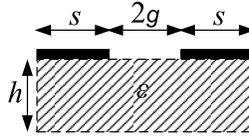
Figure 3. General form of divided structures of Fig. 2.

(a)   (b)
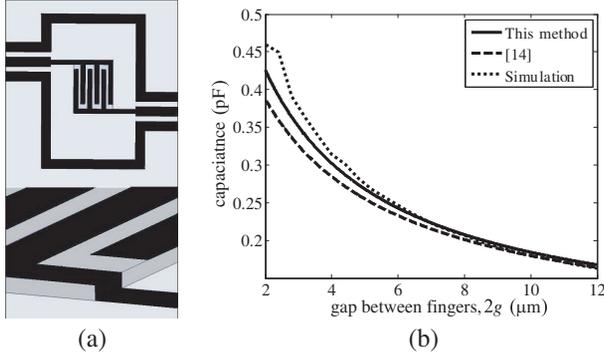
Figure 4. (a) A typical structure of an IDC, (b) C versus g.

of analysis, a typical IDC structure of Fig. 4(a) is adopted from [14], where the structural parameters are given as, $2s = 2g_e = 2w = 8\,\mu\text{m}$, $\ell = 60\,\mu\text{m}$, $n = 6$, $\varepsilon_2 = 250$, $h_2 = 2\,\mu\text{m}$, $\varepsilon_1 = 9.8$, $h_1 = 200\,\mu\text{m}$. The results of our method of analysis, method of [14] and simulation results by Ansoft HFSS are presented in Fig. 4(b), which clearly reveals the accuracy of our analytical method.

2.2. Effective Length of the Fringing Capacitor

In order to account for the non-regular field distribution regions near the corners at the end of fingers, Ref. [14] suggests the substitution of $2s$ with $\ell_f = 2s + \pi s$. we have used the same criteria in obtaining the results of Fig. 4(b). However, to be more accurate, we notice that the length of the fringing capacitor is, in fact, a function of g, g_e and s, as

$$\ell_f = 2s + \pi s f_1(g, s) f_2(g_e, s) \tag{2}$$

Assuming $f_2(g_e, s) = 1$ for $g_e = s$, our results in Fig. 4(b) would coincide with simulation results if the function $f_1(g, s)$ is chosen as, $f_1(g, s) = \sqrt{s/g}$. The results is shown in Fig. 5(a). Now, having $f_1(g, s)$, the function $f_2(g_e, s)$ is assumed to be a quadratic function as $a_1(\frac{g_e}{s})^2 + a_2 \frac{g_e}{s} + a_3$. Then, the unknown parameters a_1, a_2 and a_3 are
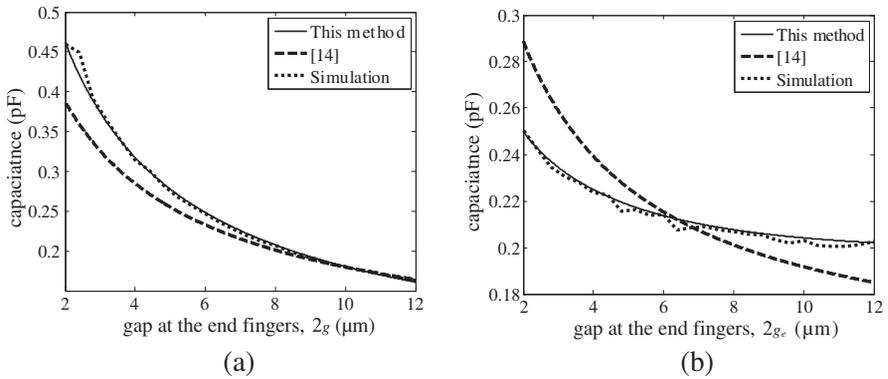
Figure 5. (a) Capacitance versus g for $g_e = s$. (b) Capacitance versus g_e for $g = s$.
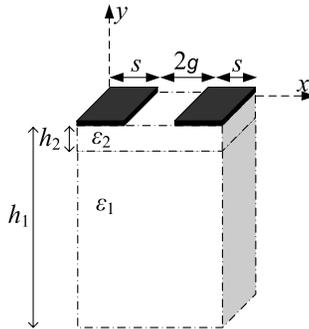
Figure 6. Layout of periodic section.

calculated such that the results of theory and simulation to be in close agreement for different values of g_e:

$$\ell_f = 2s + \pi s \sqrt{\frac{s}{g} \left(\frac{1}{10} \left(\frac{g_e}{s} \right)^2 + \frac{11}{20} \frac{g_e}{s} + \frac{7}{20} \right)} \tag{3}$$

The developed criteria was applied to the example of Fig. 4(a), and its accuracy is demonstrated in Fig. 5(b).

3. RELATION OF THE FIELD AND RELATIVE PERMITTIVITY OF THE FERROELECTRIC WITH APPLIED VOLTAGE

The layout of a periodic section of an IDC is shown in Fig. 6. The theory to determine the electric field distribution is explained in

Appendix B. According to [15], the relative permittivity of the layer under the gap between two strips has the main role in calculating the capacitance. Therefore, in this work, the relative permittivity would be computed at middle point of the two strips and $0.5\,\mu m$ away from them, and would be assigned as relative permittivity of the whole ferroelectric layer. Although, the relative permittivity of ferroelectric is dependent on the applied voltage, but the E-V relationship in ferroelectric layer remains almost constant for large values of ε_2 (r.f. Appendix B). Therefore, we assume a large value for ε_2 and obtain the E-V relation.

The computed and simulated x and y components of the electric field in ferroelectric layer (region 2) at two different distances away from the strips are represented in Fig. 7. From Fig. 7, the field at the middle of gap and distance of $0.5\,\mu m$ away, is seen to be; $E_x = 0.191\,V/\mu m$ and $E_y = 0$. Therefore, for the specific dimensions given in Fig. 7 a linear relation between E-V can be written as,

$$E = 0.191 \times 10^{-6} V \tag{4}$$

In Appendix C, a formula for relating the relative permittivity of BST-0.5 to the applied electric field is developed, which along with (4) provides the relationship of the relative permittivity and the applied voltage between fingers. This dependency is computed and shown in Fig. 8.
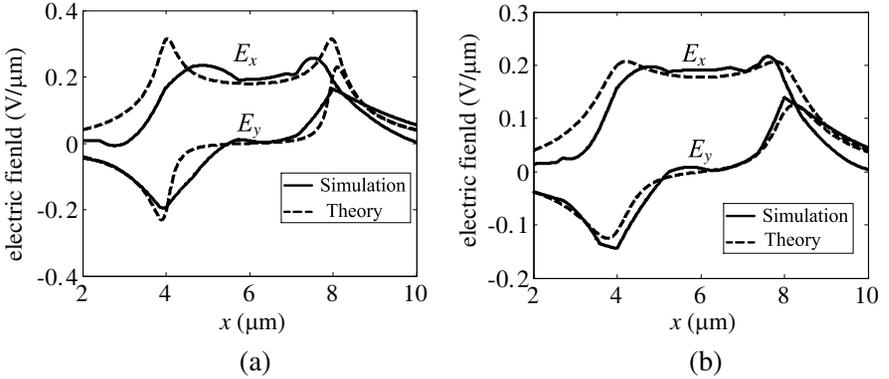
Figure 7. Electric field components with $s = 2g = 4\,\mu m$, $\varepsilon_2 = 250$, $\varepsilon_1 = 9.8$, $h_2 = 2\,\mu m$, $h_1 \gg h_2$. (a) $0.2\,\mu m$ away from strips. (b) $0.5\,\mu m$ away from strips.
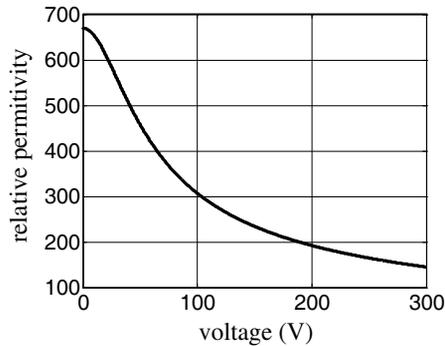
Figure 8. Dependency of the relative permittivity of BST-0.5 with thickness of $2\,\mu\text{m}$ to the applied voltage between fingers, assuming $T = 300\,\text{K}$.

Table 1. Values of the elements of the unit cell.

	a (nH)	b (pF)	c (pF)	d (nH)	L_c (nH)	c_c (pF)
set I	1.38	0.14	0.33	0.59	-	-
set II	1.38	0.14	-	0.59	0.1	0.28

4. DESIGN PROCEDURE FOR A MODIFIED CRLH UNIT CELL

In order to use only one bias network for each unit cell, the shunt inductors of the conventional CRLH unit cell are moved to end points, while their values are multiplied by two. The resultant configuration is shown in Fig. 9. The unknown parameters a, b, c and d are determined such that the center frequency has the value of 11.45 GHz and the Bloch impedance is $Z_B = 50\,\Omega$. Also, we must have the balanced condition. The frequency of 11.45 GHz is chosen since it is in the ku-band and in middle of the up-link satellite communication band (11.2–11.7 GHz) [16]. The resultant parameters, called set I parameters, are shown in Table 1. To implement elements, ferroelectric IDC is used for capacitors and spiral inductor for inductors. In conventional CRLH unit cell the parallel capacitor is a parasitic element. However, in our proposed unit cell, due to structural considerations, it is created by an IDC in parallel branch.

The layout of an IDC was shown in Fig. 1. The layout of a spiral inductor is depicted in Fig. 10, where ℓ_1, ℓ_2, w, s, and n are length of first outermost segment, length of second outermost segment, conductor width, conductor spacing, and number of turns,
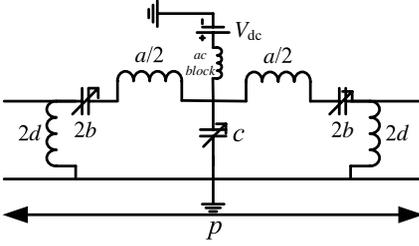
Figure 9. Circuit model of the modified CRLH unit cell.
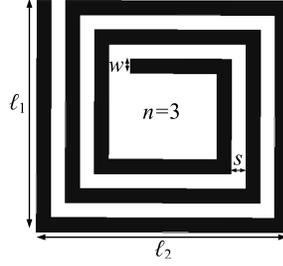
Figure 10. Layout of a spiral inductor.

respectively. In order to design the series ferroelectric IDC of Fig. 9 with $2b = 0.28\,\text{pF}$, we use the analytical method of Section 2 to obtain the initial values of the structure parameters, then obtained analytical values for dimensions of the IDC are used as initial values in simulation and the length of IDC is varied until the desired value of $2b = 0.28\,\text{pF}$ is obtained. The IDC can be modelled with a series capacitor of capacitance $2b$ and a series inductor of inductance L_{series}, therefore the required inductor in series branch of unit cell may be found as,

$$L_r = \frac{a}{2} - L_{series} = 0.61\,\text{nH} \tag{5}$$

The elements are simulated individually to reach the related values. The dimensions of these elements are shown in Table 2 with subscript i.

To confirm the accuracy of the designed elements, we determine their values in a configuration that they are connected to each other. To relate the element values to Y or Z parameters, the structure is converted to Π or T models, respectively. For Π-model, the parallel capacitor is removed from the unit cell and the dimensions are varied until the desired parameter values of set I are achieved. The dimensions of these elements are shown in Table 2 with subscript u. To complete the unit cell design, the parallel capacitor is added to the Π-model and its length is varied until the balanced condition is achieved. The final length of the unit cell is obtained $p = 0.55\,\text{mm}$.

In fact, the designed parallel capacitor is comprised of a series connection of capacitor c_c and inductor L_c. To determine L_c and c_c, the parallel inductors are removed from the unit cell, which leaves a T-model. Then, L_c and c_c are determined from Z-parameters which their values at $11.45\,\text{GHz}$ would be $L_c = 0.1\,\text{nH}$ and $c_c = 0.28\,\text{pF}$. Using these values instead of c in set I parameters gives new parameters called set II that are added to Table 1. Bloch equivalents, i.e., β_B and Z_B,

Table 2. Comparison the dimensions of elements.

		$2b_t$	$2b_i$	$2b_u$	c_i	c_u
	$2s\,(\mu\mathrm{m})$	8	8	8	8	8
	$2g\,(\mu\mathrm{m})$	4	4	4	4	4
capacitors	$2g_e\,(\mu\mathrm{m})$	8	8	8	8	8
	$2w\,(\mu\mathrm{m})$	8	8	8	8	8
	$\ell\,(\mu\mathrm{m})$	50	51	48	42	33
	n	6	6	6	6	6

		L_{r_i}	L_{r_u}	$2d_i$	$2d_u$	d_i	d_u
	$\ell_1\,(\mu\mathrm{m})$	121	121	139	127	112	127
	$\ell_2\,(\mu\mathrm{m})$	121	121	139	127	127	137
inductors	$w\,(\mu\mathrm{m})$	8	8	8	8	8	8
	$s\,(\mu\mathrm{m})$	8	8	8	8	8	8
	n	1.5	1.5	2.5	2.5	1.5	1.5

can be obtained from S-parameters. For symmetrical and reciprocal unit cell [17]:

$$Z_B = \sqrt{\frac{B}{C}}; \qquad \cos(\beta_B p) = A \qquad (6)$$

where p is the length of one unit cell. Converting ABCD parameters to S-parameters yields,

$$Z_B = Z_0 \sqrt{\frac{(1+S_{11})^2 - S_{12}^2}{(1-S_{11})^2 - S_{12}^2}}; \qquad \beta_B p = \arccos\left(\frac{1 - S_{11}^2 + S_{12}^2}{2S_{12}}\right) \quad (7)$$

The designed unit cell and Bloch equivalents are shown in Fig. 11. In Fig. 11(b) and other dispersion diagrams, an air line ($\beta = \frac{\omega}{c} = k_0$) is added in which the fast wave region is $|\beta| < k_0$.

　　Table 2 compares dimensions of the elements that are determined individually (subscripted i), and the elements that are determined in the unit cell configuration (subscripted u). For series capacitor the theoretically obtained dimensions are also included with subscript t. In this table, the dimensions of d_u are extracted from 3-unit cell configuration.

　　This table shows that the series elements are well matched but not the parallel elements, which is due to ignoring the coupling effects of the parallel inductors with ground strips and this is the reason of discrepancy between simulation and circuit model results.

(a)

(b)

(c)
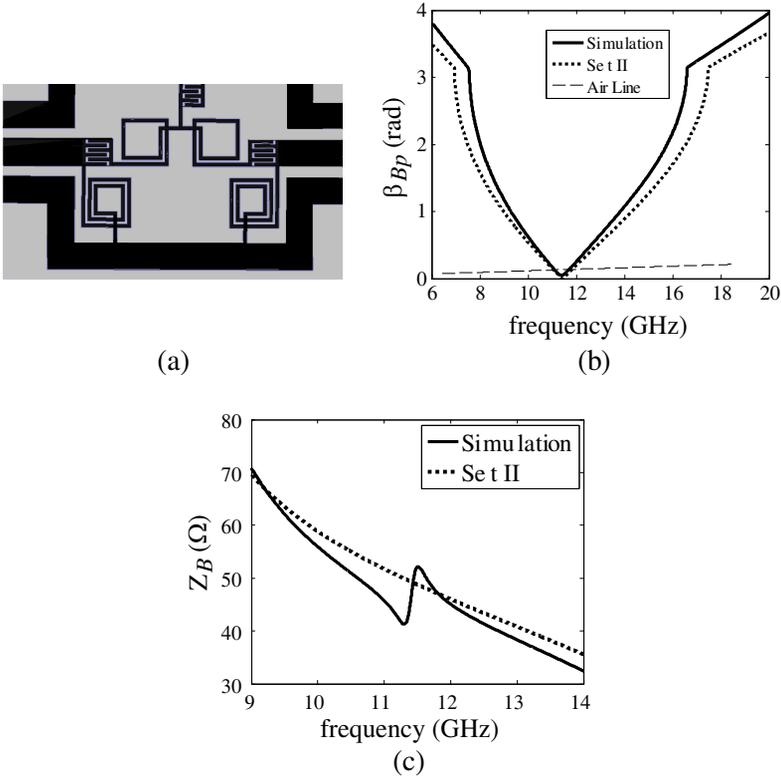
Figure 11. Designed unit cell and Bloch equivalents obtained from circuit model using set II parameters and simulation. (a) Designed unit cell. (b) Bloch propagation constant. (c) Bloch impedance.

5. PERIODICAL STRUCTURE

Interconnection of the designed unit cells to create a periodic structure, leads to a leaky-wave antenna. In the periodic structure, two parallel inductors with the value of $2d = 1.18\,\text{nH}$ which are created at connections, can be replaced by one with the value of $d = 0.59\,\text{nH}$. The designed element d, is inserted into periodic structure and its length is varied to achieve the minimum insertion loss. Fig. 12 illustrates three unit cell configuration. The propagation constant, β and attenuation factor, α of a network TL of the length ℓ can be computed from the transmission parameter as [7]:

$$\beta = -\phi(S_{12})/\ell \, ; \quad \alpha = -\ln|S_{12}|/\ell \tag{8}$$

In a lossless LWA, the leakage factor, α_{rad}, is approximately equal to the attenuation factor, α.
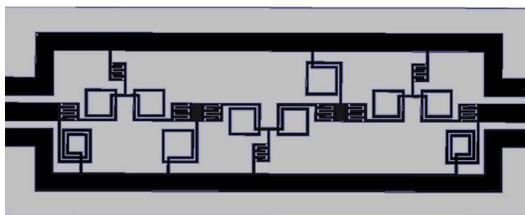
Figure 12. Three unit cells.
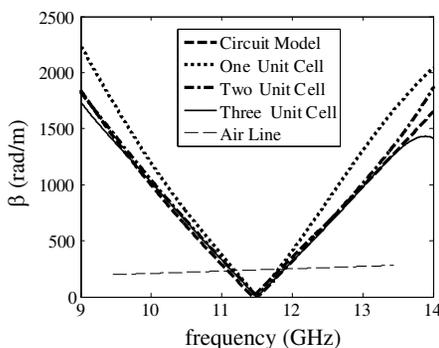
Figure 13. β of circuit model using parameters set II (theory) and various unit cell structures (simulation).

Table 3. Values of analysing 3-unit cell.

V (Volts)	145	140.7	136.6	131.9	128.8	125.3	121.8
ε	240	245	250	256	260	265	270
α (Np/m)	6.2	6.2	6.6	6.2	7.6	7	9.6
β (rad/m)	-192	-130.9	-64.4	0.2	65.5	114	209

Propagation constant, β, of circuit model using parameters set II (theory), one, two and three unit cell structures (simulation) are compared in Fig. 13. This figure represents good agreement between circuit model and periodic structure results, as the number of unit cells are increased. This is achieved by inserting the inductor, d in periodic structure in order to compensate for coupling effects that result in deviations of parallel inductor values, $2d$, from those of unit cell. The convergence rate of the β obtained from circuit model to that of two or three unit cell configurations, suggests its usage in structures that are composed of more unit cells, as well.
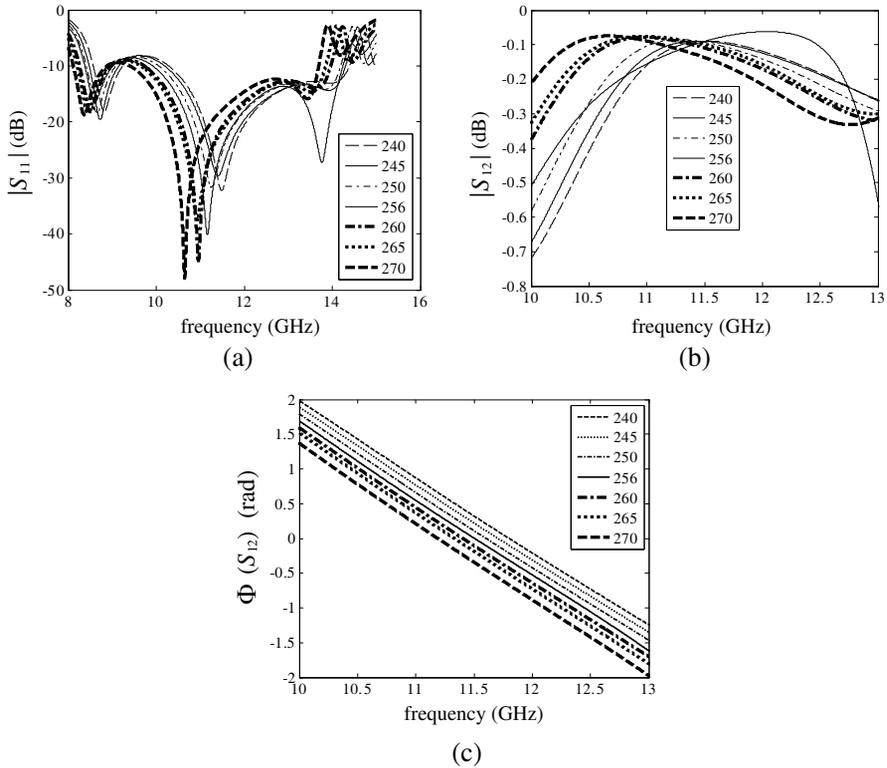
Figure 14. Investigation of 3-unit cell structure parameters variation with various relative permittivities of the ferroelectric layer. (a) Magnitude of S_{11}. (b) Magnitude of S_{12}. (c) Phase of S_{12}.

Figure 14 represents S_{11}, S_{12} and $\phi(S_{12})$ of 3-unit cell configuration for various relative permittivities of ferroelectric IDC. Each relative permittivity corresponds to a voltage that is applied to the electrodes of the IDC of Fig. 8. For each relative permittivity, α and β per unit length, at the central frequency, are calculated using (8) and data of Figs. 14(b) and (c) and shown in Table 3.

The beamwidth and direction of a pattern are determined by α and β. For $\varepsilon_2 = 256$ the structure has the propagation constant of equal to zero at 11.45 GHz and the proposed LWA radiates at broadside. For lower relative permittivity, the propagation constant is negative at 11.45 GHz, therefore the antenna radiates at backward direction and for higher relative permittivity, the propagation constant is positive at 11.45 GHz, therefore the antenna radiates at forward direction.

6. CONCLUSION

To design an IDC with multilayered structure, a simplified method based on physical insight was proposed. Furthermore a formula was derived for the effective length of fringing capacitor. The electric field was determined by assigning the voltage between two strips in the periodic section of the IDC. By substituting the electric field with voltage in a phenomenological model, the dependency of the relative permittivity of the BST-0.5 on voltage was obtained. Finally, periodic structure, comprised of the modified CRLH unit cells, was constructed and BST-0.5 IDCs was incorporated along the structure. Tunability of the periodic structure using BST-0.5 IDCs was demonstrated by varying the relative permittivity of the BST-0.5 IDCs.

APPENDIX A.

Here, we present a calculation method of the capacitance per unit length of the periodic section. As it was mentioned in Section 2, the defined magnetic walls at both ends in Fig. 3, can be moved to infinity. Also, considering the electric field lines, an electric wall can be assumed at middle of the gap between strips. The resultant structure is shown in Fig. A1(a). Fig. A1(b) represents half of the structure of Fig. A1(a), which is drawn in complex z-plane, and has the capacitance that is twice of Fig. A1(a). To calculate the capacitance of the structure of Fig. A1(b), the following conformal mapping procedure is used. The function

$$t = \cosh^2\left(\frac{\pi z}{2h}\right) \tag{A1}$$

maps the dashed region of z-plane to the upper half of the t-plane of Fig. A1(c). The following Schwartz-Christoffel transformation maps the upper half of the t-plane to the inside of rectangular region in w-plane (Fig. A1(e)):

$$\frac{dw}{dt} = \frac{A}{\sqrt{(t - t_1)(t - t_2)(t - t_3)(t - t_4)}} \tag{A2}$$

Now, consider the following transformation [18]:

$$u = \sqrt{\frac{t - t_1}{t - t_4}\frac{t_2 - t_4}{t_2 - t_1}} \tag{A3}$$

Therefore,

$$\frac{dw}{dt} = \frac{dw}{du}\frac{du}{dt} = \frac{A'}{\sqrt{(1 - u^2)(1 - k^2 u^2)}}\frac{du}{dt} \tag{A4}$$
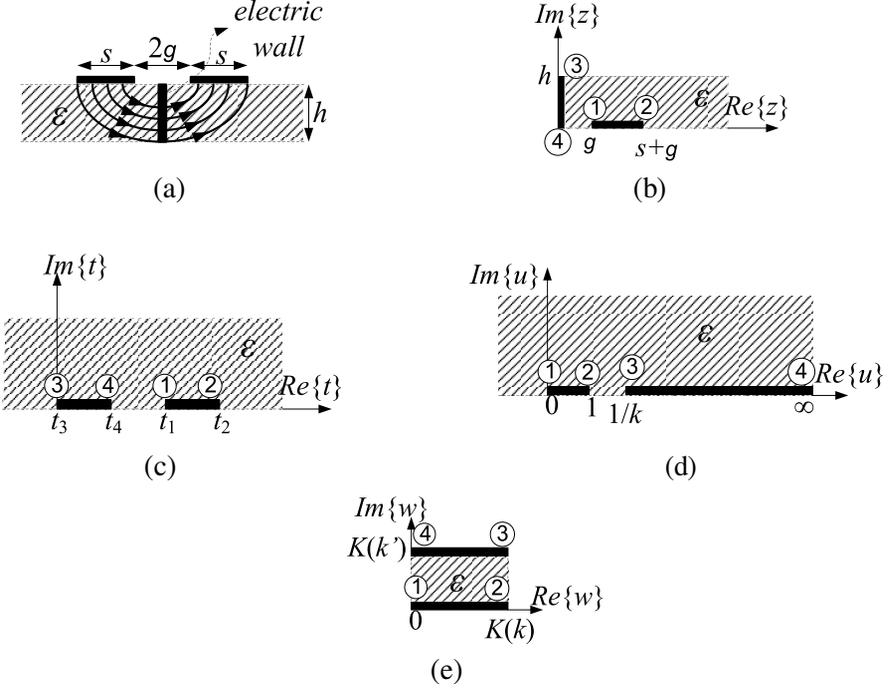
Figure A1. Process of calculating periodical section capacitance.

where

$$k = \sqrt{\frac{t_3 - t_4}{t_3 - t_1} \frac{t_2 - t_1}{t_2 - t_4}} \tag{A5}$$

and

$$A' = \frac{2A}{\sqrt{t_2 - t_4}\sqrt{t_3 - t_1}} \tag{A6}$$

In fact (A3) transforms the t-plane of Fig. A1(c) to the u-plane of Fig. A1(d), and the function

$$w = \int_0^u \frac{A'}{\sqrt{(1 - u^2)(1 - k^2 u^2)}} \, \mathrm{d}u + B \tag{A7}$$

maps the u-plane to the w-plane of Fig. A1(e) with $A' = 1$ and $B = 0$. The integral of the form (A7) is an elliptical integral of the first kind and $K(k)$ is the complete elliptic integral [19], with the modulus k given in (A5) and $k' = \sqrt{1 - k^2}$.

The capacitance per unit length in Fig. A1(e) is:

$$C = \varepsilon_0 \varepsilon \frac{K(k)}{K(k')} \tag{A8}$$

Consequently, the total capacitance of periodic section C_n is:

$$C_n = (n-3)\frac{\ell}{2}\varepsilon_0 \left[(\varepsilon_1 - 1)\frac{K(k_1)}{K(k_1')} + (\varepsilon_2 - \varepsilon_1)\frac{K(k_2)}{K(k_2')} + 2\frac{K(k_3)}{K(k_3')} \right] \tag{A9}$$

where k_i's are obtained from Eq. (A5) as,

$$\begin{cases} k_i = \dfrac{\sqrt{1 - \sinh^2(\frac{\pi g}{2h_i})/\sinh^2(\frac{\pi(s+g)}{2h_i})}}{\cosh(\frac{\pi g}{2h_i})}, & i = 1,2 \\ k_3 = \sqrt{1 - (\frac{g}{s+g})^2}, & i = 3 \end{cases} \tag{A10}$$

with

$$t_1^{(i)} = \cosh^2(\frac{\pi g}{2h_i}) \; ; \; t_2^{(i)} = \cosh^2\left(\frac{\pi(s+g)}{2h_i} \right)$$
$$t_3^{(i)} = 0 \; ; \; t_4^{(i)} = 1 \qquad i = 1,2,3 \tag{A11}$$

and $i = 1, 2$ and 3 are referring to the regions with the relative permittivity of $\varepsilon_1 - 1$, $\varepsilon_2 - \varepsilon_1$ and 1, respectively, according to Fig. 2.

APPENDIX B.

Referring to Fig. A1(e), the electric field can easily be found as,

$$E_w = \varepsilon_0 \varepsilon \frac{V/2}{K(k')} \tag{B1}$$

where V is the voltage between two strips and, therefore, the voltage between one strip and the electric wall is $V/2$.

The electric field in the physical plane (z-plane) is defined as,

$$E_z = E_w \frac{dw}{dz} = E_w \frac{dw}{dt} \frac{dt}{dz} \tag{B2}$$

Substituting for dw/dt from Eq. (A2) and dt/dz from Eq. (A1), the partial electric field can be calculated as,

$$E_{zi} = \varepsilon_0 \varepsilon \frac{V/2}{K(k_i')} \frac{1/2\sqrt{t_2^{(i)} - t_4^{(i)}}\sqrt{t_3^{(i)} - t_1^{(i)}}}{\sqrt{(t - t_1^{(i)})(t - t_2^{(i)})(t - t_3^{(i)})(t - t_4^{(i)})}}$$
$$\times \frac{\pi}{2h_i} \sinh(\frac{\pi z}{h_i}) \; ; \quad i = 1,2,3 \tag{B3}$$

where k_i' and $t^{(i)}$ are defined in Eqs. (A10) and (A11) by considering $k_i' = \sqrt{1 - k^2}$. According to partial displacement method, the electric field in layer 2 is:

$$E_2 = E_{2x} + jE_{2y} = \frac{1}{\varepsilon_0 \varepsilon_2}((\varepsilon_1 - 1)E_{z1} + (\varepsilon_2 - \varepsilon_1)E_{z2} + E_{z3}) \quad (B4)$$

where E_{zi} is defined in Eq. (B3).

APPENDIX C.

In the paraelectric phase, the relative permittivity of ferroelectrics are high and depends on temperature, external electric field and mechanical stress [20]. Solid solutions $Ba_x Sr_{1-x} TiO_3$ are in paraelectric phase at room temperatures. A phenomenological model proposed by Vendik and Zubko depicts the dependency of relative permittivity on temperature and electric field. In paraelectric phase for $Ba_x Sr_{1-x} TiO_3$, we have:

$$\varepsilon(E, T) = \frac{\varepsilon_{00}}{f} \quad (C1)$$

where,

$$f = (a + \xi(E))^{2/3} + (a - \xi(E))^{2/3} - \eta(T); \quad a = [\xi(E)^2 + \eta(T)^3]^{.5}$$
$$\xi(E) = \sqrt{(E/E_N)^2 + \xi_s^2}; \quad \eta(T) = \sqrt{(\theta_F/4T_C)^2 + (T/T_C)^2} - 1$$
$$E_N = 2D_N/[\varepsilon_0 (3\varepsilon_{00})^{3/2}]; \quad \varepsilon_{00} = C/T_C$$

This model is valid for bulk single crystals.

For a thin film, the size effect should also be taken into account [21], as

$$\frac{1}{\varepsilon_{eff}} = \frac{1}{\varepsilon} + \frac{2}{\alpha h} \quad (C2)$$

where, ε_{eff} is the effective relative permittivity of the film, ε is the relative permittivity of the bulk material determined from (C1), h is the film thickness and α is related to correlation parameter λ_1 as; $\alpha = 1/\sqrt{2\lambda_1}$. The model parameters for the $Ba_{0.5} Sr_{0.5} TiO_3$ (BST-0.5) are given in Table C1.

Table C1. Model parameters for $Ba_{.5} Sr_{.5} TiO_3$.

T_C (K)	θ_F (K)	D_N (C/m^2)	E_N (kV/cm)	ε_{00}	ξ_s	α (μm)$^{-1}$
245	175	4.2	225	400	0.3	1400

REFERENCES

1. Caloz, C., T. Itoh, and A. Rennings, "CRLH metamaterial leaky-wave and resonant antennas," *IEEE Antennas and Propagation Magazine*, Vol. 50, No. 5, 25–39, Oct. 2008.

2. Yu, A., F. Yang, and A. Elsherbeni, "A dual band circularly polarized ring antenna based on composite right and left handed metamaterials," *Progress In Electromagnetics Research*, Vol. 78, 73–81, 2008.

3. Anghel, A. and R. Cacoveanu, "Improved composite right/left-handed cell for leaky-wave antenna," *Progress In Electromagnetics Research Letters*, Vol. 22, 59–69, 2011.

4. Liu, C. Y., Q. X. Chu, and J. Q. Huang, "Double-side radiating leaky-wave antenna based on composite right/left-handed coplanar-waveguide," *Progress In Electromagnetics Research Letters*, Vol. 14, 11–19, 2010.

5. Abdelaziz, A. F., T. M. Abuelfadl, and O. L. Elsayed, "Leaky wave antenna realization by composite right/left-handed transmission line," *Progress In Electromagnetics Research Letters*, Vol. 11, 39–46, 2009.

6. Kodera, T. and C. Caloz, "Uniform ferrite-loaded open waveguide structure with CRLH response and its application to a novel backfire-to-endfire leaky-wave antenna," *IEEE Trans. on Microw. Theory and Tech.*, Vol. 57, No. 4, 784–795, Apr. 2009.

7. Caloz, C. and T. Itoh, *Electromagnetic Metamaterials: Transition Line Theory and Microwave Applications*, John Wiley and Sons Inc., 2006.

8. Lim, S., C. Caloz, and T. Itoh, "Metamaterial-based electronically controlled transmission-line structure as a novel leaky-wave antenna with tunable radiation angle and beamwidth," *IEEE Trans. on Microw. Theory and Tech.*, Vol. 53, No. 1, 161–173, Jan. 2005.

9. Abdalla, M. A. Y., K. Phang, and G. V. Eleftheriades, "A planar electronically steerable patch array using tunable PRI/NRI phase shifters," *IEEE Trans. on Microw. Theory and Tech.*, Vol. 57, No. 3, 531–541, Mar. 2009.

10. Bahl, I., *Lumped Elements for RF and Microwave Circuits*, Artech House Inc., 2003.

11. Nath, J., D. Ghosh, J. Maria, A. I. Kingon, W. Fathelbab, P. D. Franzon, and M. B. Steer, "An electronically tunable microstrip bandpass filter using thin-film Barium-Strontium-Titanate (BST) varactors," *IEEE Trans. on Microw. Theory and*

Tech., Vol. 53, No. 9, 2707–2711, Sep. 2005.

12. Yildiz, C., K. Guney, M. Turkmen, and S. Kaya, "Neural models for coplanar strip line synthesis," *Progress In Electromagnetics Research*, Vol. 69, 127–144, 2007.

13. Marynowski, W., P. Kowalczyk, and J. Mazur, "On the characteristic impedance definition in microstrip and coplanar lines," *Progress In Electromagnetics Research*, Vol. 110, 219–235, 2010.

14. Gevorgian, S., T. Martinsson, L. J. P. Linnér, and E. L. Kollberg, "CAD models for multilayered substrate interdigital capacitors," *IEEE Trans. on Microw. Theory and Tech.*, Vol. 44, No. 6, 896–904, Jun. 1996.

15. Carlsson, E. and S. Gevorgian, "Conformal mapping of the field and charge distributions in multilayered substrate CPWs," *IEEE Trans. on Microw. Theory and Tech.*, Vol. 47, No. 8, 1544–1552, Aug. 1999.

16. Volakis, J. L., *Antenna Engineering Handbook*, 4th edition, McGraw-Hill Co., 2007.

17. Pozar, D. M., *Microwave Engineering*, 3rd edition, John Wiley and Sons Inc., 2005.

18. Gevorgian, S., L. J. P. Linnér, and E. L. Kollberg, "CAD models for shielded multilayered CPW," *IEEE Trans. on Microw. Theory and Tech.*, Vol. 43, No. 4, 772–779, Apr. 1995.

19. Schinzinger, R. and P. A. A. Laura, *Conformal Methods and Applications*, Dover Publications, 2003.

20. Gevorgian, S., *Ferroelectrics in Microwave Devices, Circuits and Systems*, Springer-Verlag Co., 2009.

21. Vendik, O. G. and S. P. Zubko, "Ferroelectric phase transition and maximum dielectric permittivity of displacement type ferroelectrics $(Ba_xSr_{1-x}TiO_3)$," *Journal of Applied Physics*, Vol. 88, No. 9, 5343–5350, Nov. 2000.